Volume 3 | Number 34 | 14 September 2015 | Pages 17481–17882

Journal of Materials Chemistry A

Materials for energy and sustainability

www.rsc.org/MaterialsA

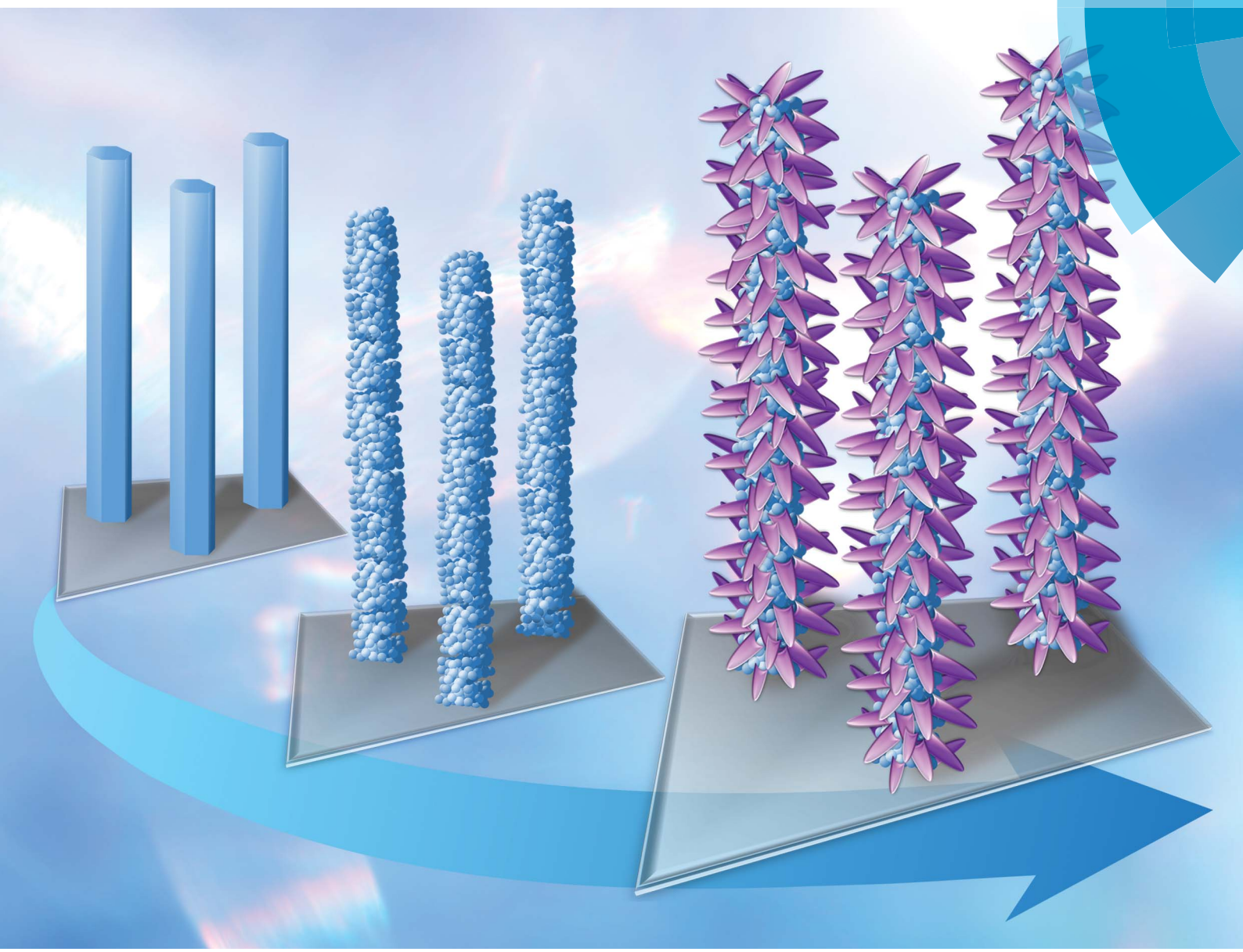

ISSN 2050-7488

ROYAL SOCIETY OF CHEMISTRY

PAPER

D. Mattia *et al.*

Hierarchical 3D ZnO nanowire structures *via* fast anodization of zinc

Journal of Materials Chemistry A

PAPER

View Article Online
View Journal | View Issue

Cite this: J. Mater. Chem. A, 2015, 3, 17569

Hierarchical 3D ZnO nanowire structures *via* fast anodization of zinc†

D. O. Miles,[a] P. J. Cameron[b] and D. Mattia*[c]

Received 15th May 2015
Accepted 23rd June 2015

DOI: 10.1039/c5ta03578c

www.rsc.org/MaterialsA

ZnO nanowire structures are used today in a variety of applications, from gas/chemical sensing to photocatalysis, photovoltaics and piezoelectric actuation. Electrochemical anodization of zinc foil allows rapid formation of high aspect ratio ZnO nanowires under mild reaction conditions compared to more common fabrication methods. In this study we demonstrate, for the first time, how 3D hierarchical ZnO nanowire structures can be fabricated by controlling the type of electrolyte and anodization voltage, temperature and time. Optimization of the reaction conditions yields growth rates of up to 3.2 μm min^{-1} and the controlled formation of aligned arrays of nanowires, flower-like nanostructures, and hierarchical, fractal nanowire structures. Annealing of the nanowires produces high surface area (55 m^2 g^{-1}) nanowires with slit-type pores perpendicular to the nanowire axis. In depth analysis of the anodization process allows us to propose the likely growth mechanisms at work during anodization. The findings presented here not only contribute to our knowledge of the interesting area of zinc anodization, but also enable researchers to design complex hierarchical structures for use in areas such as photovoltaics, photocatalysis and sensing.

1. Introduction

ZnO has proven to be an incredibly versatile material, finding application in many areas including gas/chemical sensing, photocatalysis, photovoltaics and piezoelectrics.[1–4] Among its beneficial properties are a wide band gap (3.37 eV), allowing absorption in the UV region, and a high electron mobility.[5] Perhaps one of the most inviting features of ZnO to the materials community, however, is the wide range of micro and nanostructured morphologies it can be produced in.[6]

One of the most interesting nanostructures of ZnO for many applications is the nanowire. Ordered arrays of nanowires can be grown on a variety of different substrates using techniques including chemical vapour deposition, atomic layer deposition, hydrothermal growth and sol–gel chemistry to name but a few.[7–10] However, growth of nanowires using these techniques typically encounters one of two potential problems: (1) growth proceeds at high temperatures, limiting the choice of substrate and often requiring costly experimental setups, or (2) growth occurs at a very low rate, thereby requiring reaction times on the scale of hours or even days to gain sufficient nanowire lengths.

One class of techniques that can be used to avoid these two issues is electrochemical growth, which typically occurs at temperatures below 100 °C and can proceed at a high rate to give aligned nanowire films. Electrodeposition is the primary example of this class of techniques and has been used extensively for the growth of ZnO nanowires; reviews of which can be found in the literature.[11,12] Over the past few years however, another electrochemical technique has emerged for the production of ZnO nanostructures, based on electrochemical anodization of metallic zinc.

Electrochemical anodization is the process of oxidising the surface of a metal (the anode) under an applied voltage resulting in the formation of a variety of nanostructures. It is a well-established technique for metals such as aluminium where it has found a wide range of applications.[13,14] Other metals such as titanium, zirconium, niobium and hafnium have also been successfully anodized, all forming either organised nanoporous or nanotubular morphologies.[15–18]

The anodization of zinc has received relatively little attention compared to other metals. One reason for this is likely to be the instability of zinc and its oxide form in the acidic electrolytes commonly used during anodization. On the other hand, nanostructures including nanostripes, nanowires, nanodots and nanoflowers have all been produced using electrolytes ranging from basic NaOH solutions to highly protic HF solutions.[19–23]

[a]Centre for Sustainable Chemical Technologies, University of Bath, Bath, BA2 7AY, UK
[b]Department of Chemistry, University of Bath, Bath, BA2 7AY, UK
[c]Department of Chemical Engineering, University of Bath, Bath, BA2 7AY, UK. E-mail: D.Mattia@bath.ac.uk; Tel: +44 (0)1225 383961

† Electronic supplementary information (ESI) available: FESEM surface morphologies and cross-sections for nanowire films grown at different times, temperatures, voltages and electrolyte concentrations are provided. Additional structural characterisation including FT-IR and particle size analysis. FESEM surface morphologies of nanowire film damage resulting from either high voltages or the annealing process. Typical current–time data from anodization. See DOI: 10.1039/c5ta03578c

One of the most interesting anodization systems reported has been that by Hu *et al.* who were able to form ZnO nanowires with aspect ratios exceeding 1000 *via* anodization in $KHCO_{3(aq.)}$ followed by annealing.[20] The attractive features of this technique have not been left unnoticed and have been applied in the production of nanowires for both dye-sensitized solar cells (DSSCs) and photodetectors.[24–26] A study of the early stages of this growth has also been examined under both potentiostatic and galvanostatic conditions by Choi *et al.*[27]

In this investigation we present a significant advance, both in our understanding and control of this anodization system. We demonstrate, for the first time, that rapid growth of nanowires can be achieved using a range of different bicarbonate electrolytes to produce aligned nanowire arrays, flower-like nanostructures and hierarchical structures. We also report optimised growth rates of up to 3.2 μm min^{-1} by controlling the reaction conditions. Through annealing the nanowires we obtain unique polycrystalline structures with slit-like pores which can also be further modified to give hierarchical structures. These materials, which combine a one-dimensional structure with a high surface area, could be promising within applications such as photovoltaics, photocatalysis and sensing.

2. Experimental

2.1 Materials

Ethanol (96%), sodium bicarbonate (99.7–100.3%), potassium bicarbonate (99.7%), ammonium bicarbonate (≥99.0%) and acetone (≥99.5%) were purchased from Sigma-Aldrich. Perchloric acid (60–62%) and zinc foil (0.25 mm thickness, 99.98%) were purchased from Alfa Aesar. Deionised water was used throughout all experiments and obtained from a Millipore system at a resistivity of >18.2 MΩ cm.

2.2 Preparation of anodic nanowires

Zinc foils were annealed at 300 °C for 1 hour in air followed by degreasing with acetone in an ultrasonic bath for 10 minutes. The degreased zinc foils were electropolished at 10 V for 15 minutes in an electrolyte consisting of a 1 : 4 volumetric ratio of perchloric acid and ethanol at −70 °C under rapid stirring to produce a mirrored finish (Fig. S1†). After electropolishing the zinc foil was washed with ethanol and deionised water to remove any remaining electrolyte from its surface.

The electropolished zinc foil was applied as the anode in a two-electrode cell with a stainless steel plate held parallel to the anode at a distance of 10 mm acting as the cathode. The active area of the zinc anode was controlled using a specially designed Teflon® sample holder which exposed three circular areas (each 12 mm diameter) on one face of the zinc foil. The anodization was conducted in an aqueous electrolyte of either $KHCO_3$, $NaHCO_3$ or NH_4HCO_3 (0.05–0.20 mol dm^{-3}) with constant stirring. The temperature of the electrolyte was controlled (5–20 °C) using a jacketed beaker linked to a refrigerated circulating bath. Anodizations were undertaken for different lengths of time (1–120 min) at a constant voltage (1–10 V) provided by a DC power supply (Agilent, E3634A). After anodization, the anodic films were washed thoroughly with deionised water to remove any excess electrolyte from the surface. The foils were then dried under a gentle flow of argon gas and stored within a desiccator until they were characterised. To gain polycrystalline ZnO nanowires the anodic films were annealed at 300 °C for 1 h in air using a ramping rate of 1 °C min^{-1}. Further modification of the ZnO nanowires to form hierarchical nanostructures was achieved by first leaving the annealed films in a sealed vial containing deionised water for 24 h. The films were then rinsed with deionised water, dried under a flow of argon and annealed at 300 °C for 1 h.

2.3 Materials characterisation

Surface morphologies and cross-sectional morphologies of the as-prepared anodic films were examined using a field emission scanning electron microscope (FESEM, JEOL, JSM6301F). Cross-sections were obtained by cutting through the anodic films and bending the foil in order to cleave the edge of the nanowire film from the zinc substrate. Average film thicknesses were measured *via* analysis of the FESEM micrographs within ImageJ using five separate measurements at regular intervals along the cross-section, the error of which is represented as the standard deviation. Transmission electron microscopy (TEM) was performed using a Philips CM200 FEGTEM. Prior to TEM analysis the nanowires were scraped from the substrate and dispersed *via* sonication in ethanol.

X-ray diffraction (XRD) measurements were recorded for the as-prepared and annealed anodic films using a Bruker D8-Advance set in flat plate mode. Fourier transform infra-red (FT-IR) spectra of the anodic nanostructures produced by anodization were recorded using a Perkin-Elmer Spectrum 100 FT-IR spectrometer operating between 4000–600 cm^{-1}. X-ray photoelectron spectroscopy (XPS) of the as-prepared and annealed nanowire films was performed using a VG Escalab 250.

3. Results and discussion

3.1 Key stages of nanowire growth

3.1.1 Initiation of nanowire growth. In contrast to electrodeposition, where a zinc precursor such as zinc acetate is present within the electrolyte solution, Zn^{2+} ions must first be sourced from the zinc anode *via* dissolution. In the very early stages of anodization this proceeds *via* the dissolution of the anode to form small, discrete pits over the surface of the metal, which can be observed *via* SEM (Fig. 1a). This initial dissolution stage can be observed within the recorded current–time plot as an initial surge in current to what will be the current maximum for the anodization (Fig. S2†). After this stage the current can be observed to start a steady decrease. It is at this point that nanowire growth commences. Nanowire growth first proceeds *via* the formation of discrete bladed structures which we will term as nanoflowers (Fig. 1b). Through SEM analysis it appears that nanoflower growth occurs near to, or indeed from within, the number of small pits formed from dissolution, assumedly due to the localized high concentration of Zn^{2+} ions. In these early stages of growth

the multiple one-dimensional protrusions that make up the nanoflower more closely resemble blades than nanowires, with tips that taper to a point. Over these early stages of anodization growth continues to proceed both by the increase in quantity of nanoflowers over the surface and increase in the size of the nanoflowers, with growth proceeding in an ever enlarging hemisphere centred at the point of initiation. This has been demonstrated schematically in stages 1–3 in Fig. 1c.

3.1.2 Formation of aligned nanowire films. The next phase of growth sees the morphology transform from discrete nanoflower structures to a uniform film of aligned nanowires. SEM analysis reveals that this transition likely occurs simply *via* inhibited growth of nanowires that are directed parallel, or close to parallel, with the anode surface. This physical inhibition, due to overcrowding and competition for space between neighbouring nanoflowers, can be observed in Fig. 2a and b where the ideal hemispherical shape of one nanoflower is overlapping with its neighbour. Under these conditions growth is hindered parallel to the substrate but can proceed freely in a direction perpendicular to the substrate, leading to gradual alignment of nanowires, which is demonstrated in stages 4 & 5 within Fig. 1c. Further crowding and overlap near to the anode eventually leads to the formation of a relatively dense bottom layer, at which point the morphology can be considered as a uniform nanowire film (Fig. 2c).

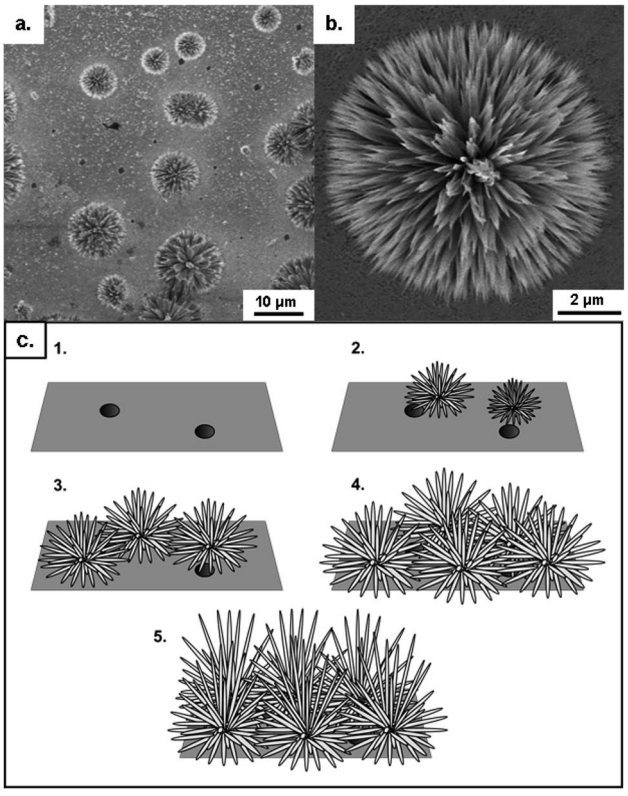

Fig. 1 FESEM micrographs of multiple (a) and a single nanoflower (b) formed in the early growth stages and graphical representation of the initial stages of nanowire growth (c).

3.1.3 Layered and hierarchical growth. For a period of time following the alignment phase, growth of nanowires proceeds vertically, as might be expected, with little evidence of nanowire widening. Nanowire diameters of approximately 100–150 nm can be observed in Fig. 3a, which was typical of films in the earlier stages of growth. After a time, however, it could be clearly observed *via* SEM that much wider wire structures (300–1000 nm) emerged from the top of the relatively uniform nanowire film. These wires displayed a clear hexagonal structure (Fig. 3b) that was not observed with the smaller nanowires and appeared to grow at a faster rate. This led to the formation of a layered cross-section of the film, with an upper layer of large hexagonal wires above a more densely packed layer of smaller nanowires (Fig. 3c).

A further peculiarity in the anodization was also observed in the form of hierarchical growth. The initiation of this hierarchical growth process is shown to occur *via* the branching of a single large, hexagonal wire into several smaller nanowires, with diameters similar to those at the start of nanowire growth (Fig. 3d–f). These smaller nanowires, together with the underlying wires, can continue growing to form very thick nanowire films (>100 μm). At thicknesses in excess of 50 μm however, complex 3D networks of nanowires were typically formed rather than aligned nanowires.

The exact reasons for both the formation of layered films of different sized nanowires and the formation of hierarchical structures are currently unknown. This could be related to the increasing distance from the source of Zn^{2+} ions to the nanowire tip, thereby reducing the concentration of Zn^{2+} ions available for reaction. It might also be attributed to a decreasing concentration of the already dilute bicarbonate species present in the electrolyte as a function of time.

3.2 Control of nanowire growth

In the initial report on this anodization system by Hu *et al.*, the influence of the temperature, time and voltage on the surface morphology was examined using SEM.[20] These experiments highlighted some interesting features of the anodic growth, including the formation of spherical and lamellar structures at high temperatures (50–70 °C), and also cracking of films at elevated voltages (~40 V) due to oxygen evolution beneath the nanowire films. Although these qualitative insights provided an excellent starting point in understanding this unusual growth, further quantitative measurements of the factors controlling the growth of nanostructures are necessary to be able to design bespoke hierarchical nanostructures for specific applications.

In this section we examine in detail the effect of altering the conditions of voltage, temperature and time on nanowire growth and also examine the previously unstudied effects of electrolyte concentration and type. In order to gain quantitative information on growth rates under different conditions we measured the cross-sectional film thickness, corresponding to the nanowire length, *via* FESEM.

Although previous investigations in this area have reported the formation of nanowires in an aqueous $KHCO_3$ electrolyte, we in fact found that this growth was also possible when either sodium or ammonium bicarbonate electrolytes were used.

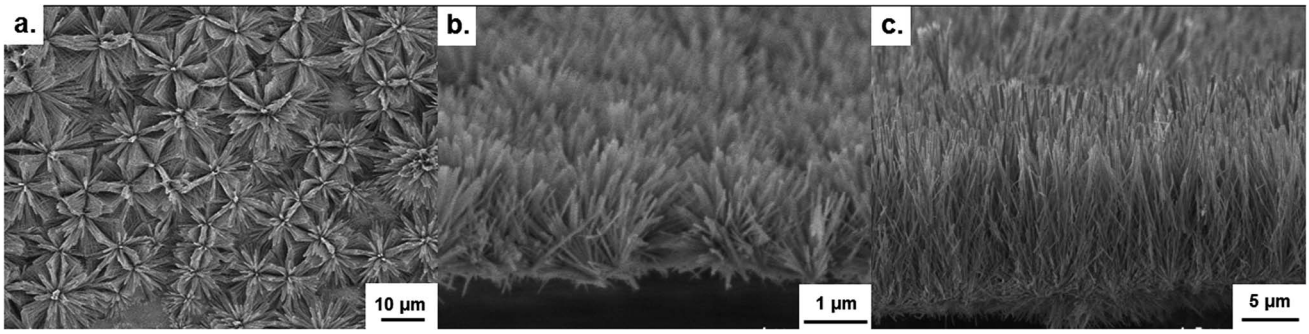

Fig. 2 FESEM surface morphology (a) and cross-section (b) showing the complete coverage of the zinc surface with nanoflowers resulting in the alignment of nanowires (c).

In both cases the nanowire growth rates were found to be significantly higher than those previously reported for anodizations in a potassium bicarbonate electrolyte.[20,24] The major steps of growth presented in the previous section were found to be independent of the bicarbonate species used with only slight variations in growth rates. Therefore, in this section we present only the results from the two novel anodizations in the sodium and ammonium bicarbonate electrolytes.

3.2.1 Effect of time on growth. The effect of time on nanowire growth was investigated by fixing the voltage, electrolyte concentration and temperature at 5 V, 50 mM and 10 °C respectively whilst anodizing for different lengths of time, between 1 and 120 minutes. As might be expected, longer anodization times led to longer nanowires, as shown in the SEM surface morphologies (Fig. 4), cross-sections (Fig. S3†) and graphically in Fig. 5. The evolution of a layered cross-section, with wider nanowires appearing between 5 and 15 minutes, is apparent in the case of both electrolytes, as discussed in the previous section. Only slight deviations in film thickness are obtained between the two electrolytes, with growth in the NH_4HCO_3 electrolyte appearing to slow over time, perhaps due to slow depletion of the electrolyte species.

3.2.2 Effect of voltage on growth. Variation of the applied voltage between 1 and 10 V, whilst keeping all other reaction conditions constant at 10 °C, 50 mM electrolyte concentration and 15 minutes anodization time, resulted in a significant effect on nanowire growth rates. Whilst homogenous nanowire films were formed in the case of the anodizations at 2 and 5 V, incomplete coverage was observed for 1 V and severe cracking and flaking of the film was observed at 10 V (Fig. S4†). By plotting the measured film thicknesses against the anodization voltage (Fig. 5) it can be observed that it obeys a non-linear trend. A likely reason for this is due to the detachment of sections of the cracked film during anodization at the highest

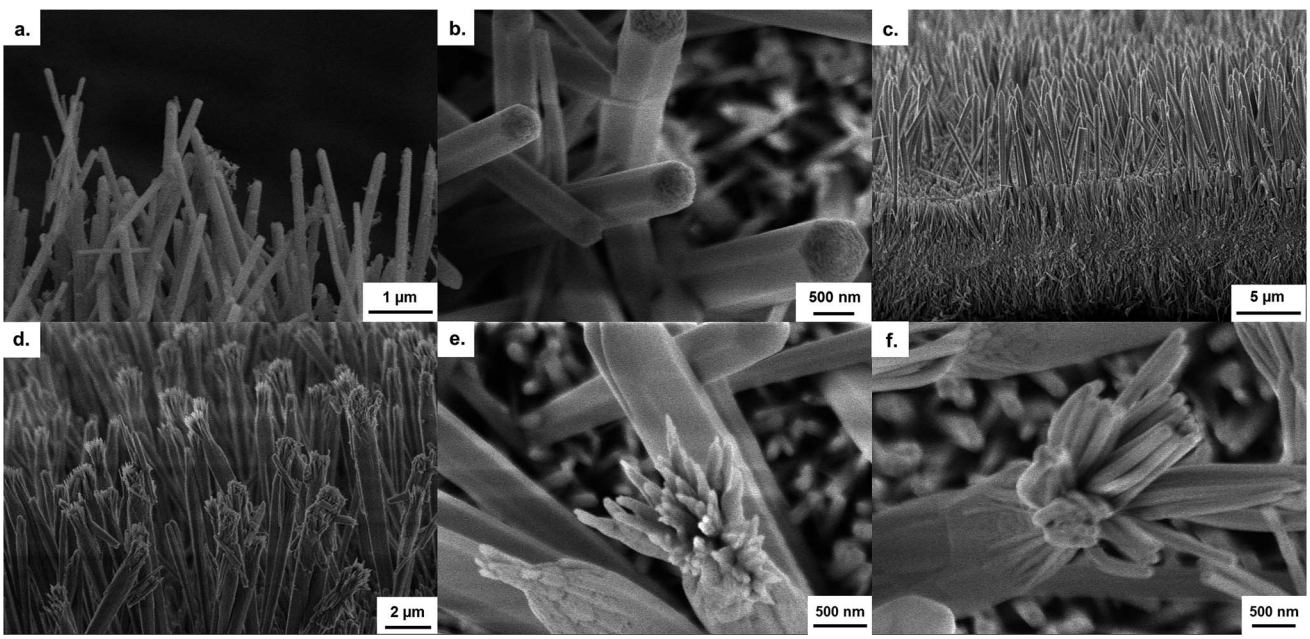

Fig. 3 FESEM cross-sections and surface morphologies showing the initial formation of thin nanowires (a), the development of a layered structure with large hexagonal wires (b & c) and the formation of hierarchical structures (d–f).

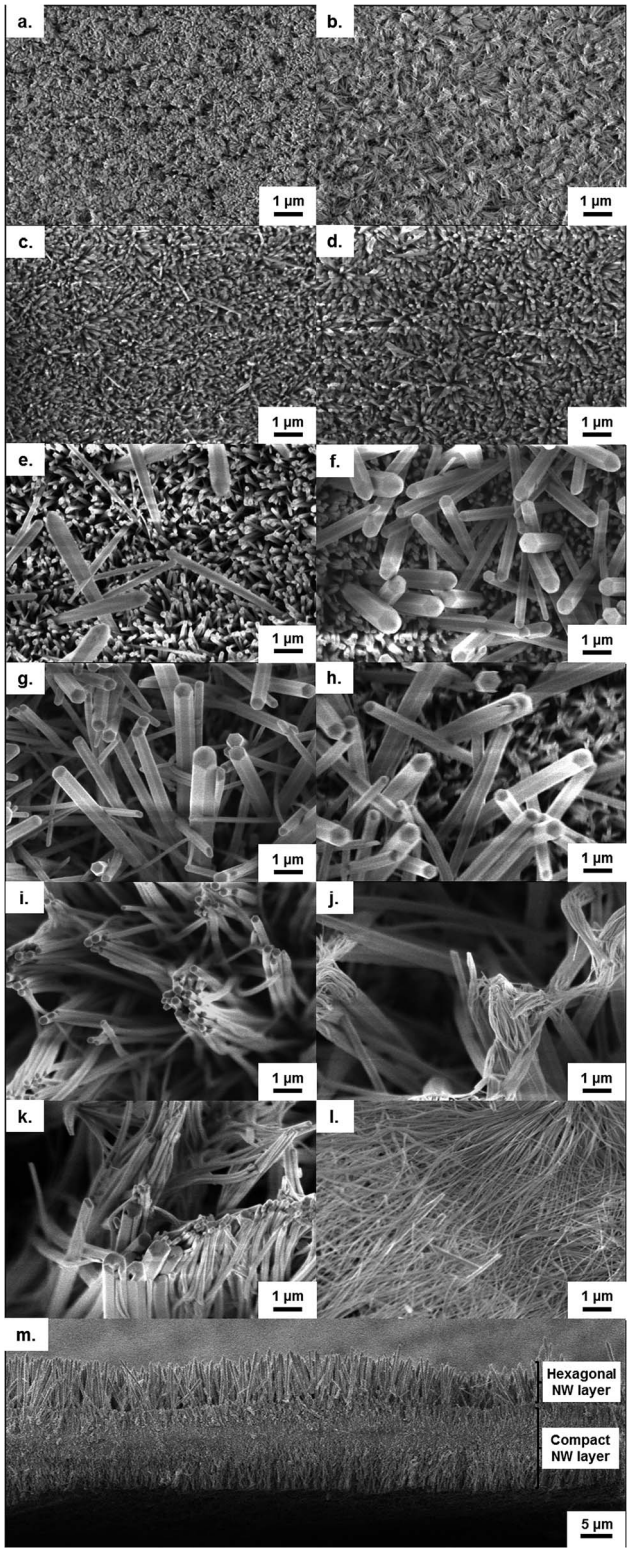

Fig. 4 FESEM surface morphologies of nanowire (NW) films formed after anodizations for 1 (a & b), 5 (c & d), 15 (e & f), 30 (g & h), 60 (i & j) and 120 minutes (k & l) in aqueous $NaHCO_3$ and NH_4HCO_3 electrolytes respectively. Representative FESEM cross-section (m) corresponding to NW film shown in (f).

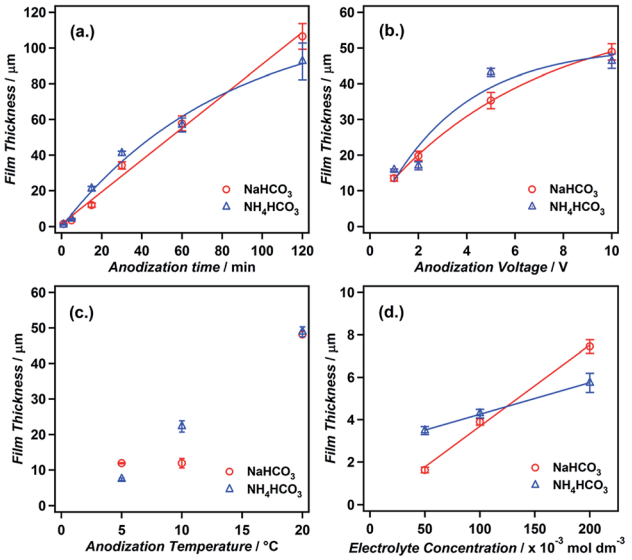

Fig. 5 Nanowire film thicknesses obtained from FESEM for anodizations undertaken for different times (a) and at different voltages (b), temperatures (c) and electrolyte concentrations (d). Conditions used were 15 min, 5 V, 10 °C and 50 mM electrolyte concentration for (a–c) and 2 V, 10 °C and 5 minutes for (d).

voltages. This cracking was also observed by Hu *et al.* for anodizations in $KHCO_3$ when high voltages were used (40 V).[20] This was attributed to oxygen evolution beneath the film, which can then rupture the film upon its escape (Fig. S5†). It should be noted that this cracking occurs at a lower voltage than reported by Hu *et al.* using our experimental setup. This can be explained by the decreased electrode separation used in this study, which can significantly alter the current when a low concentration, and therefore high resistivity, electrolyte is used.

As homogeneous nanowire films are typically desired for applications, it is therefore important for researchers applying this technique to both select suitable voltages (2–5 V) as well as carefully control the electrochemical cell setup in order to gain reproducible results.

3.2.3 Effect of temperature on growth. By examining the cross-sections of the films formed at different temperatures for the $NaHCO_{3(aq.)}$ and $NH_4HCO_{3(aq.)}$ electrolytes (Fig. S6†), it can clearly be observed that the reaction temperature has a significant effect on the rate of nanowire growth. Within the plot of the typical film thicknesses against the reaction temperature (Fig. 5) it can be seen that growth rate can be increased by approximately five times by a temperature increase of just 15 °C. The results show a linear trend, with the exception of an anomalous result for the $NaHCO_3$ electrolyte at 10 °C, which can possibly be attributed to film damage after anodization. The use of near ambient temperatures (20 °C) allowed extremely high nanowire growth rates of 3.2 μm min^{-1} to be achieved. These growth rates are significantly higher than those previously reported for anodization of zinc in a $KHCO_3$ electrolyte, which were 0.5 and 1.3 μm min^{-1}.[20,24] These high growth rates were achieved without causing damage to the film, which is observed when applying high voltages. We therefore propose that the

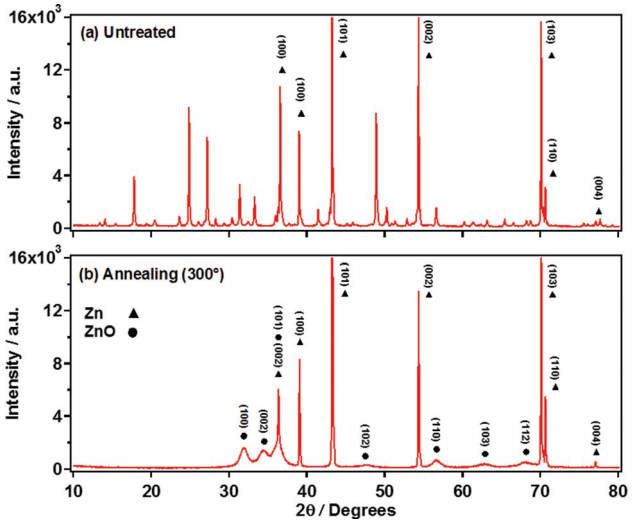

Fig. 6 Flat plate powder XRD patterns for nanowire films obtained directly from anodization (a) and after annealing at 300 °C for 1 h (b).

anodization temperature is a more useful parameter to control in order to alter the growth rate of nanowire films.

3.2.4 Effect of electrolyte concentration on growth. To investigate the effect of electrolyte concentration on nanowire growth the voltage, temperature and anodization time were fixed at 2 V, 10 °C and 5 minutes respectively whilst varying the concentration between 50 and 200 mM. A combination of higher voltage (5 V) and higher concentration resulted in significant fracturing and flaking of the anodic film, similarly to what was observed using anodization voltages of 10 V. Using a lower voltage (2 V) it was possible to obtain more accurate film thickness trends without the inaccuracies presented by a damaged film. SEM cross-sections of the films (Fig. S7†) and a plot of film thickness *vs.* concentration (Fig. 5) reveal that the concentration also had a significant effect on the rate of nanowire growth. Analysis of the surface morphologies revealed that even though a low voltage was used, cracking was present in the film at 200 mM electrolyte concentrations. This signifies that similarly to increasing the voltage, increases in growth rate can be obtained, but at the expense of the film integrity, which is of importance for application of the nanowire films. In light of this, we again propose that temperature might be a more useful variable in controlling the growth rate of the nanowire films using this anodization system.

3.3 Rationalising the rapid nanowire growth

To make sense of the unusually rapid nanowire growth observed for such mild conditions, it was first important to try and establish the chemical structure of the nanowires in order to hypothesise possible formation mechanisms. The original study by Hu *et al.* postulated that the material formed from anodization in $KHCO_3$ could be of the form $Zn(CO_3)_n(OH)_m$, due to the main anions present in the solution being OH^- and CO_3^{2-}.[20] Subsequent studies on anodization carried out under similar conditions have described the nanowires prior to annealing as being composed of either $Zn(OH)_2$ or ZnO but with little evidence to support this.[26,27]

Powder X-ray diffraction (pXRD) patterns of the nanowire films prior to annealing display a complex set of sharp peaks, indicating a highly crystalline material (Fig. 6). This is consistent with the observation of smooth hexagonal nanowires *via* FESEM. The peaks were not found to match with either ZnO, $Zn(OH)_2$ or $ZnCO_3$ and neither were they found to match with known hydroxy carbonates of zinc, $Zn_5(CO_3)_2(OH)_6$ and $Zn_4CO_3(OH)_6\cdot H_2O$. Given the complex nature of the pattern, it is possible that a mixture of these materials could be present.

The X-ray photoelectron spectrum of the as-prepared nanowire film reveals a significant quantity of carbon present in addition to the expected zinc and oxygen (Fig. 7). A small quantity of iron could also be detected, which is likely to originate from the stainless steel counter electrode in the anodization setup. Analysis of the C1s region of the X-ray photoelectron spectrum reveals two peaks: a peak at lower energy attributed to adventitious carbon contamination, and a peak at slightly higher energy within the region often attributed to a metal carbonate. The latter peak is slightly shifted to higher energy compared to a typical metal carbonate which is consistent with a hydrocarbonate species.[28] Since no peaks attributable to Na 1s are present it can be assumed that the hydrocarbonate peak is not due to remaining $NaHCO_3$ from the electrolyte.

The FT-IR spectrum of the as-prepared material (Fig. S8†) also indicates the presence of carbonate and hydroxide ions, strengthening the hypothesis that the nanowires consist of a form of zinc hydroxy carbonate.

The aqueous chemistry of the zinc cation can be relatively complex with dependence on many factors including the pH, temperature, concentration and presence of other anions. The

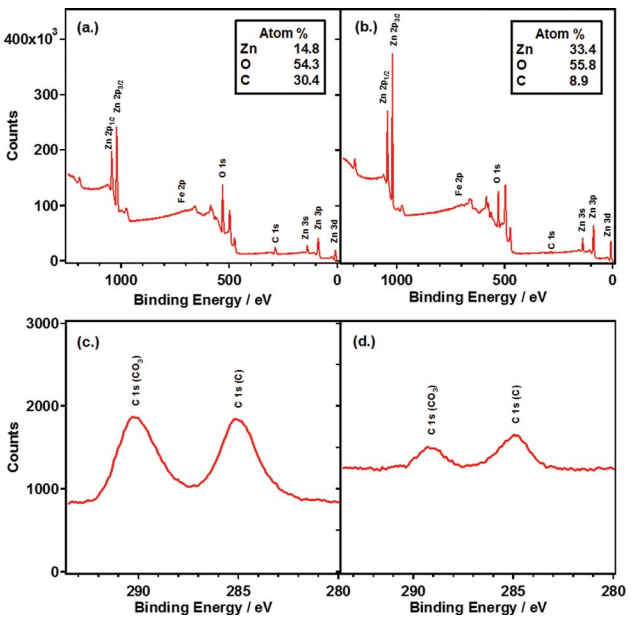

Fig. 7 XPS survey spectra and C1s region spectra for nanowire films obtained directly from anodization (a & c) and after annealing at 300 °C (b & d).

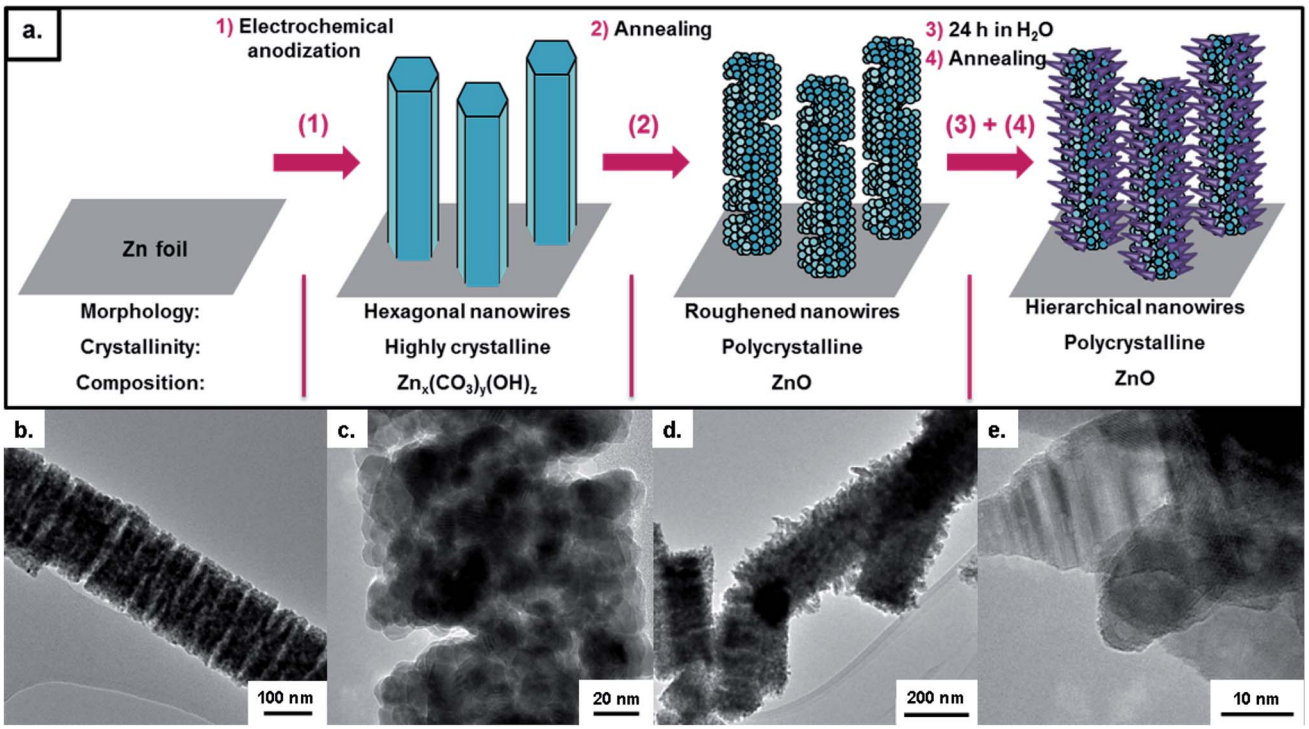

Fig. 8 Scheme showing the two step production of polycrystalline ZnO nanowires with a "slit-pore" structure and further modification to hierarchical structures (a). TEM micrographs of the "slit-pore" nanowires (b & c) and hierarchical structures (d) with a magnified micrograph of the ZnO horns (e).

route to zinc hydroxy carbonate formation in aqueous solutions has been previously discussed by Orel *et al.* on the basis of a partial charge model.[29,30] In water, zinc can form the relatively stable hydrated ions $[Zn(OH_2)_6]^{2+}$ and $[Zn(OH)(OH_2)_5]^{+}$, which can condense to form $[Zn(OH)_2(OH_2)_4]$ *via* olation and oxolation mechanisms. In the presence of HCO_3^-, either through dissolved CO_2, or in our case through the bicarbonate electrolyte, substitution of up to two water molecules can occur to give $[Zn(OH)(HCO_3)(OH_2)_3]$. Fast condensation of this species *via* the olation mechanism will then yield a zinc hydroxy carbonate. Based on this, we believe that the anodization could proceed *via* the following reactions:

At the anode.

$$Zn_{(s)} + 6H_2O \rightarrow [Zn(OH_2)_6]^{2+} + 2e^- \quad (1)$$

$$[Zn(OH_2)_6]^{2+} \leftrightarrow [Zn(OH)(OH_2)_5]^{+} + H^+ \quad (2)$$

$$[Zn(OH)(OH_2)_5]^{+} + HCO_3^- \leftrightarrow [Zn(OH)(HCO_3)(OH_2)_3] + 2H_2O \quad (3)$$

$$[Zn(OH)(OH_2)_5]^{+} \leftrightarrow [Zn(OH)_2(OH_2)_4] + H^+ \quad (4)$$

$$x[Zn(OH)_2(OH_2)_4] + y[Zn(OH)(HCO_3)(OH_2)_3] \rightarrow [Zn_{x+y}(OH)_{2x}(CO_3)_y] + 4(x+y)H_2O \quad (5)$$

At the cathode.

$$2H^+ + 2e^- \rightarrow H_{2(g)} \quad (6)$$

Condensation rates *via* the olation mechanism can proceed rapidly, sometimes being only limited by diffusion.[31] As we have good mixing due to stirring we can assume that this reaction is not mass transfer limited, leading to rapid nanowire growth. With the reduction of protons at the cathode (reaction (6)) it would be expected that reaction (2) would be driven forwards, accelerating the overall condensation. An increase in concentration of the bicarbonate electrolyte would also be expected to drive forward reaction (3), explaining the observed trend of increased growth rate at higher concentrations. This all contributes towards explaining the rapid growth of nanowires observed in this anodization reaction.

3.4 Conversion to ZnO and further modifications

Annealing of the nanowire films was found to yield polycrystalline ZnO. This can be observed through the broad peaks in the X-ray diffraction patterns corresponding to the wurzite form of ZnO (Fig. 6b). Although the overall nanowire form was preserved during annealing, the nanowires' facets were no longer smooth, but instead formed of multiple small nanoparticles with a "slit-pore" structure along the length of the nanowires (Fig. 8b and c). Particle sizes were determined to be 9 ± 2 nm as determined by TEM, and were found to be dependent on the annealing temperature (Fig. S9†). This interesting polycrystalline "slit-pore" structure contributes significantly towards a high specific surface area of 54.4 $m^2\ g^{-1}$, similar to values for much smaller (<25 nm) nanoparticle powders. This high surface area, combined with the one-dimensional

structure, makes these materials interesting candidates for applications such as dye-sensitized solar cells.

An insight into the formation of this porous structure can be gained by considering the structural transformation occurring during annealing. Using the assumption that the as-prepared nanowires are a form of zinc hydroxy carbonate then degradation to ZnO will proceed *via* the loss of H_2O and CO_2.[32] Using the case of hydrozincite ($Zn_5(CO_3)_2(OH)_6$) as an analogy, the decomposition reaction proceeds as:

$$Zn_5(CO_3)_2(OH)_6 \rightarrow 5ZnO + 3H_2O + 2CO_2 \quad (7)$$

Loss of these two gases during heating results in a contraction between the plains of the remaining Zn and O atoms to form ZnO. As there is a higher number density of Zn atoms in the ZnO than the hydrozincite, void formation is inevitable. A decomposition such as this can explain the formation of a porous polycrystalline structure as presented here. This contraction can also be used to explain an often unwanted side-effect of the annealing process, which is cracking of the nanowire films. Cracking of the films during annealing was observed to some extent for all of the anodized films produced, even when low heating and cooling rates were used (Fig. S10†). This apparently unavoidable feature should be considered, particularly when the application requires a continuous, crack free film.

In addition to the "slit-pore" type structures, it was found that through a simple post-treatment interesting hierarchical structures could be obtained (Fig. 8d and e). This treatment involved leaving the nanowire film within a sealed vial of deionised water for 24 h, followed by another annealing treatment. The hierarchical structures consisted of horn shaped ZnO crystals of ~40 nm in length surrounding the existing nanowire structure. These structures are likely to be the result of a slow secondary growth of ZnO onto the nanowires with hydrated zinc ions from the substrate as the ion source. The flat plate XRD pattern and XPS spectrum of the hierarchical nanowires indicate that no substance other than ZnO are present after this treatment (Fig. S11 and S12†). This simple modification may provide a route to even higher surface area nanostructures than the nanowires with slit-type pores and would therefore also be promising candidates for application in areas such as dye-sensitized solar cells and photocatalysis.

4. Conclusions

We have been able to demonstrate for the first time that the growth of high aspect ratio nanowires *via* the anodization of zinc can be achieved using a range of different bicarbonate electrolytes. We have also been able to show quantitatively that the reaction parameters of temperature, voltage, time and electrolyte concentration can significantly alter the nanowire growth rate. By optimising these parameters, remarkably high growth rates in excess of 3 μm min^{-1} can be achieved at room temperature, without destruction of the nanowire films. Examination of the properties of the nanowire films before and after annealing have allowed us to propose an explanation, both for the high growth rates achieved, and for the unique porous structure of the annealed ZnO nanowires. Furthermore, we have been able to present a simple post-treatment of the nanowires which gives rise to interesting hierarchical structures.

The insights presented provide an important contribution towards the area of zinc anodization, an area that is currently ill-understood. Knowledge of the factors controlling the process, and the mechanisms underpinning them, will aid researchers in the field to design controlled hierarchical nanostructures in areas where it is likely to show promise, such as photovoltaics, photocatalysis and sensing.

Acknowledgements

The authors would like to acknowledge the Leeds EPSRC Nanoscience and Nanotechnology Research Equipment Facility (LENNF) for use of the TEM and XPS equipment. D. Miles would like to thank the EPSRC for funding through the Centre for Sustainable Chemical technologies (Grant no. EP/G03768X/1). D. Mattia would like to acknowledge the Royal Academy of Engineering for funding. All data created during this research are openly available from the University of Bath data archive at http://dx.doi.org/10.15125/BATH-00078.

Notes and references

1 A. Wei, L. H. Pan and W. Huang, *Mater. Sci. Eng., B*, 2011, **176**, 1409–1421.
2 M. D. Hernandez-Alonso, F. Fresno, S. Suarez and J. M. Coronado, *Energy Environ. Sci.*, 2009, **2**, 1231–1257.
3 Q. F. Zhang, C. S. Dandeneau, X. Y. Zhou and G. Z. Cao, *Adv. Mater.*, 2009, **21**, 4087–4108.
4 B. Kumar and S.-W. Kim, *Nano Energy*, 2012, **1**, 342–355.
5 D. C. Look, D. C. Reynolds, J. R. Sizelove, R. L. Jones, C. W. Litton, G. Cantwell and W. C. Harsch, *Solid State Commun.*, 1998, **105**, 399–401.
6 C. Klingshirn, J. Fallert, H. Zhou, J. Sartor, C. Thiele, F. Maier-Flaig, D. Schneider and H. Kalt, *Phys. Status Solidi B*, 2010, **247**, 1424–1447.
7 E. Galoppini, J. Rochford, H. Chen, G. Saraf, Y. Lu, A. Hagfeldt and G. Boschloo, *J. Phys. Chem. B*, 2006, **110**, 16159–16161.
8 K. Subannajui, F. Guder, J. Danhof, A. Menzel, Y. Yang, L. Kirste, C. Y. Wang, V. Cimalla, U. Schwarz and M. Zacharias, *Nanotechnology*, 2012, **23**, 235607–235613.
9 L. E. Greene, M. Law, J. Goldberger, F. Kim, J. C. Johnson, Y. F. Zhang, R. J. Saykally and P. D. Yang, *Angew. Chem., Int. Ed*, 2003, **42**, 3031–3034.
10 S. E. Ahn, J. S. Lee, H. Kim, S. Kim, B. H. Kang, K. H. Kim and G. T. Kim, *Appl. Phys. Lett.*, 2004, **84**, 5022–5024.
11 H. Zeng, J. Cui, B. Cao, U. Gibson, Y. Bando and D. Golberg, *Sci. Adv. Mater.*, 2010, **2**, 336–358.
12 M. Skompska and K. Zarebska, *Electrochim. Acta*, 2014, **127**, 467–488.
13 A. M. M. Jani, D. Losic and N. H. Voelcker, *Prog. Mater. Sci.*, 2013, **58**, 636–704.

14 G. E. J. Poinern, N. Ali and D. Fawcett, *Materials*, 2011, **4**, 487–526.
15 G. K. Mor, O. K. Varghese, M. Paulose, K. Shankar and C. A. Grimes, *Sol. Energy Mater. Sol. Cells*, 2006, **90**, 2011–2075.
16 H. Tsuchiya, J. M. Macak, I. Sieber and P. Schmuki, *Small*, 2005, **1**, 722–725.
17 I. Sieber, H. Hildebrand, A. Friedrich and P. Schmuki, *Electrochem. Commun.*, 2005, **7**, 97–100.
18 H. Tsuchiya and P. Schmuki, *Electrochem. Commun.*, 2005, **7**, 49–52.
19 S. J. Kim and J. Choi, *Electrochem. Commun.*, 2008, **10**, 175–179.
20 Z. Hu, Q. Chen, Z. Li, Y. Yu and L.-M. Peng, *J. Phys. Chem. C*, 2010, **114**, 881–889.
21 S. He, M. Zheng, L. Yao, X. Yuan, M. Li, L. Ma and W. Shen, *Appl. Surf. Sci.*, 2010, **256**, 2557–2562.
22 J. L. Zhao, X. X. Wang, J. J. Liu, Y. C. Meng, X. W. Xu and C. C. Tang, *Mater. Chem. Phys.*, 2011, **126**, 555–559.
23 A. Ramirez-Canon, D. O. Miles, P. J. Cameron and D. Mattia, *RSC Adv.*, 2013, **3**, 25323–25330.
24 Y.-T. Kim, J. Park, S. Kim, D. W. Park and J. Choi, *Electrochim. Acta*, 2012, **78**, 417–421.
25 N. Samir, D. S. Eissa and N. K. Allam, *Mater. Lett.*, 2014, **137**, 45–48.
26 S.-T. Ren, Q. Wang, F. Zhao and S.-L. Qu, *Chin. Phys. B*, 2012, **21**, 038104–038110.
27 J. Park, K. Kim and J. Choi, *Curr. Appl. Phys.*, 2013, **13**, 1370–1375.
28 A. V. Shchukarev and D. V. Korolkov, *Cent. Eur. J. Chem.*, 2004, **2**, 347–362.
29 M. Bitenc, P. Podbrscek, P. Dubcek, S. Bernstorff, G. Drazic, B. Orel, S. Pejovnik and Z. C. Orel, *Chem.–Eur. J.*, 2010, **16**, 11481–11488.
30 M. Bitenc, P. Podbrscek, P. Dubcek, S. Bernstorff, G. Drazic, B. Orel and Z. C. Orel, *CrystEngComm*, 2012, **14**, 3080–3088.
31 J. Livage, M. Henry and C. Sanchez, *Prog. Solid State Chem.*, 1988, **18**, 259–341.
32 X. Wang, W. Cai, Y. Lin, G. Wang and C. Liang, *J. Mater. Chem.*, 2010, **20**, 8582–8590.